The Astrophysical Journal, 982:160 (9pp), 2025 April 1 https://doi.org/10.3847/1538-4357/adbe37

The Radial Variation of Suprathermal Particles in Stream Interaction Regions: Comparisons between Solar Orbiter, ACE, and STEREO-A

Robert C. Allen[1], George C. Ho[1], Glenn M. Mason[2], Athanasios Kouloumvakos[2], Gang Li[3], Rachael J. Filwett[4], Maher Dayeh[1], Malik H. Walker[5], Sarah K. Vines[1], Robert F. Wimmer-Schweingruber[6], and Javier Rodriguez-Pacheco[7]

[1] Southwest Research Institute, 6220 Culebra Rd., San Antonio, TX 78238, USA
[2] The Johns Hopkins University Applied Physics Laboratory, 11101 Johns Hopkins Rd., Laurel, MD 20723, USA
[3] General Linear Space Plasma Lab LLC, USA
[4] Montana State University, Bozeman, MT 59717, USA
[5] The Johns Hopkins University, Baltimore, MD 21218, USA
[6] Institute of Experimental and Applied Physics, Christian-Albrechts-University Kiel, 24118 Kiel, Germany
[7] Universidad de Alcalá, Space Research Group, 28805 Alcalá de Henares, Spain
Received 2024 October 31; revised 2025 February 14; accepted 2025 March 5; published 2025 March 27

Abstract

With the launch of Solar Orbiter, the intensity and composition of suprathermal particles have been sampled within the inner heliosphere at distances between ∼0.3 and 1 au. This includes a multitude of observations of suprathermal ions associated with stream interaction regions (SIRs) measured by the Solar Orbiter Energetic Particle Detector, with corresponding observations at 1 au from the Ultra-Low-Energy Isotope Spectrometer on the Advanced Composition Explorer mission and the Suprathermal Ion Telescope on the Solar-Terrestrial Relations Observatory-Ahead spacecraft. Comparing observations between these spacecraft enables a statistical view of the radial variations of SIR-associated suprathermal particles, allowing for greater insight into energetic particle transport within the inner heliosphere. The observed radial trends agree well with that found by M. A. I. Van Hollebeke et al. but indicate a smaller modulation of particle spectra due to transport than predicted by L. A. Fisk & M. A. Lee. This possible difference between the observed empirical relationship and theoretical formulation may arise from either sub-Parker spiral topology in the rarefaction region and/or a velocity-dependent, rather than rigidity or explicit species-dependent, diffusion treatment in L. A. Fisk & M. A. Lee.

Unified Astronomy Thesaurus concepts: Corotating streams (314); Interplanetary physics (827)

1. Introduction

Stream interaction regions (SIRs) form where high-speed streams from equatorial coronal holes expand into preceding slow solar wind, leading to a region of compressed plasma that is often observed with associated suprathermal ion enhancements (I. G. Richardson 2004, and references therein). These ion enhancements are typically observed as dispersionless due to the spacecraft moving into prepopulated flux tubes of particles accelerated at shocks that form along the SIR, often at distances beyond 1 au (e.g., V. Pizzo 1978; L. Jian et al. 2006; L. K. Jian et al. 2008; S. A. Henderson et al. 2025). As these particles propagate sunward from the SIR-driven shock, they will experience particle scattering, adiabatic deceleration, and radial and cross-field diffusion, which will alter the particle fluence within the fluxtube (D. V. Reames 1999).

To investigate the radial dependence of suprathermal ions associated with SIRs, M. A. I. Van Hollebeke et al. (1978) compared energetic (0.96–2.2 MeV) proton peak intensities observed by Helios 1 and 2 (0.3–1 au), Interplanetary Monitoring Platform (IMP) 7 (1 au), Pioneer 11 (3.8 au), and Pioneer 10 (9–10 au). The SIRs studied by M. A. I. Van Hollebeke et al. (1978) occurred between mid-1973 and mid-1976, during the declining phase of solar cycle 20. The particle spectra associated with the SIRs were characterized by a peak in relative intensity between ∼3 and 4 au, with the intensity decreasing both toward and away from the Sun from this region. While the results from M. A. I. Van Hollebeke et al. (1978) derived an empirical relationship between the peak intensity and radial distance of SIR-associated energetic particles, the analysis was only conducted for a single energy range of protons. Early results from Solar Orbiter observations by R. C. Allen et al. (2021b), in comparison with observations from the Advanced Composition Explorer (ACE) Ultra-Low Energy Isotope Spectrometer (ULEIS), of ^{4}He at the similar rigidity as investigated by M. A. I. Van Hollebeke et al. (1978) (i.e., 226–320 keV nuc^{-1} ^{4}He versus 0.9–2.2 MeV H) found similar radial trends as those reported by M. A. I. Van Hollebeke et al. (1978).

To better understand these radial variations, the theoretical formulation by L. A. Fisk & M. A. Lee (1980) provided a framework for estimating the acceleration and transport of particles propagating away from an interplanetary shock in the heliosphere. In this framework the particle distribution function is given by

$$f = \left(\frac{r}{r_s}\right)^{2\beta/(1-\beta)+V/(\kappa_0 v)} v^{-3/(1-\beta)} \exp\left(-\frac{6\kappa_0\beta v}{V_{\rm sw}(1-\beta)^2}\right), \quad (1)$$

where r and r_s are heliocentric distances of the observer and shock, respectively, $V_{\rm sw}$ is the solar wind speed, v is the particle velocity, κ_0 is the radial diffusion coefficient from $\kappa = \kappa_0 v r$, and

$$\beta = \frac{(V'^2 + \Omega_s^2 r_s^2)^{1/2}}{V^2 + \Omega_s^2 r_s^2)^{1/2}} \frac{B}{B'}, \quad (2)$$

where V and V' is the solar wind speed upstream and downstream of the shock, respectively, B and B' is the upstream and downstream magnetic field strength, respectively, and Ω_s^2 is the angular velocity of the Sun. Using this framework for nominal solar wind parameters, G. M. Mason et al. (1999) illustrated that transport would modulate the particle spectra as they propagate back toward an observer in the inner heliosphere. This spectral modulation would lead to an increasingly lower spectral slope for low energy particles and that at sufficiently large distances from the shock, the spectra could develop a local maxima, or "rollover," in the particle spectra.

The existence of such a feature in observed SIR-associated particle spectra has not been uniformly observed. For instance, L. Zhao et al. (2016) reported the possible observation of a spectral rollover when comparing observations from Solar Terrestrial Relations Observatory-Ahead (STEREO-A) and ACE. In this study, observations from STEREO-A near a SIR-driven shock were first compared to observations at ACE, which did not observe a SIR-driven shock when the SIR crossed the spacecraft. These spectra were then compared to STEREO-A observations from within the rarefaction region behind the SIR, which would at that point be connected to the SIR-driven shock at further heliospheric distances. This comparison showed evidence of a small but notable spectral modulation between the shock spectra at STEREO-A and the ACE spectra, as well as a possible spectral rollover in the STEREO-A rarefaction region spectra (L. Zhao et al. 2016). Similarly, several SIR-associated spectra observed by Solar and Heliospheric Observatory and ACE (J. Yu et al. 2017) and STEREO (J. Yu et al. 2018) have been reported with evidence of a spectral rollover feature, becoming more pronounced and shifted to higher energies with increasing distance to the SIR-associated shock.

While these studies (L. Zhao et al. 2016; J. Yu et al. 2017, 2018) gave some indication of the predicted spectral variation with transport, other observations have reported instances where this transport-induced modulation is not observed (e.g., G. Gloeckler et al. 1979; K. Chotoo et al. 2000; M. I. Desai et al. 2020; R. C. Allen et al. 2021a; C. J. Joyce et al. 2021). M. I. Desai et al. (2020) investigated multiple SIR-associated suprathermal particle increases with Parker Solar Probe (PSP) ranging from 0.35 and 0.94 au without finding any indication of spectral modulation like predicted by L. A. Fisk & M. A. Lee (1980). Additionally, C. J. Joyce et al. (2021) investigated the temporal evolution of PSP observed suprathermal particle spectra associated with an SIR at 0.34 au. Unlike the cases reported in L. Zhao et al. (2016) and J. Yu et al. (2017, 2018), the event studied by C. J. Joyce et al. (2021) was not characterized by a spectral rollover later in the event, when presumably the spacecraft would have a significantly further path length to the SIR-driven shock. Further, R. C. Allen et al. (2021a) investigated a radially aligned SIR event between PSP (∼0.5 au) and STEREO-A (∼1 au), finding that while the average flux of suprathermal particles at PSP was lower than at STEREO-A, the spectra were only slightly modulated, significantly less than would be predicted by L. A. Fisk & M. A. Lee (1980).

This study aims to investigate, statistically, the radial variation of SIR-associated suprathermal particle fluence to better explore transport effects in the inner heliosphere. Section 2 describes the Solar Orbiter, ACE, and STEREO-A missions and data sets used in this study, along with a description of the event selection criteria. Section 3 presents the main results of the investigation, and Section 4 discusses the implications of the findings of this study.

2. Methodology

To investigate the radial variation of suprathermal particles associated with SIRs, this study utilizes suprathermal particle observations from Solar Orbiter, ACE, the STEREO-A spacecraft. To focus on times when SIRs were more likely in isolation before solar activity increased, this study only includes observations from the commissioning of Solar Orbiter in 2020 April to the beginning of 2023.

2.1. ACE

The ACE (E. C. Stone et al. 1998) mission, launched in 1997, orbits the sunward Sun–Earth Lagrange point L1. Solar wind bulk moments (velocity, density, and temperature) are taken from the Solar Wind Electron Proton Alpha Monitor (SWEPAM; D. J. McComas et al. 1998) and magnetic field observations are provided by the Magnetic Field Experiment (C. W. Smith et al. 1998). To investigate the suprathermal ion fluence at SIRs, this study uses observations from ULEIS (G. M. Mason et al. 1998), which is capable of measuring He-Ni particles with energies from $\sim$45 keV nuc^{-1} to several MeV nuc^{-1}.

2.2. STEREO-A

STEREO (M. L. Kaiser et al. 2008) was launched in 2006 October into a near-1 au orbit. While the mission originally consisted of two spacecraft, only observations from STEREO-A are available for the years investigated for this study. Bulk solar wind measurements are taken from the PLAsma and SupraThermal Ion Composition investigation (A. B. Galvin et al. 2008) and magnetic field data is from the STEREO-A magnetometer (M. H. Acuña et al. 2008). Suprathermal particle measurements are taken from the Suprathermal Ion Telescope (SIT; G. M. Mason et al. 2008), part of the In Situ Measurements of Particles and Coronal Mass Ejection (CME) Transients suite (J. G. Luhmann et al. 2008). SIT is also a time-of-flight particle instrument similar to ACE/ULEIS, allowing it to be compared to ACE/ULEIS measurements with more ease, although some care must still be taken regarding instrument sensitivity.

2.3. Solar Orbiter

Solar Orbiter (D. Müller et al. 2020) was launched in 2020 February and has since provided valuable observations of the inner heliosphere and solar corona. The perihelion of Solar Orbiter has gradually been lowered and the inclination will soon be raised out of the ecliptic through successive Venus gravity assists. During the three years of this study, the lowest perihelion reached was 0.29 au.

For Solar Orbiter, this study uses solar wind bulk plasma moments from the Proton and Alpha particle Sensor, part of the Solar Wind Analyser (C. J. Owen et al. 2020). Magnetic field observations are taken by the Solar Orbiter fluxgate vector magnetometer (T. S. Horbury et al. 2020). Suprathermal ion observations are from the Suprathermal Ion Spectrograph (SIS), part of the Energetic Particle Detector suite (J. Rodríguez-Pacheco et al. 2020; R. F. Wimmer-Schweingruber et al. 2021), which measures the suprathermal ion composition of H through Fe ions in the energy range ~0.1–10 MeV nuc^{-1}. SIS was designed after ACE/ULEIS, following a similar concept of operation and heritage, allowing for comparisons to be made between the instruments in a more straightforward fashion. This study only includes observations of ^{4}He, O, and Fe, which all three instruments (ACE/ULEIS, STEREO-A/SIT, and Solar Orbiter/SIS) can resolve reliably. Further, this study includes only observations from SIS-A, which is the sunward-directed telescope of Solar Orbiter/SIS and is most compatible to the sunward-directed ACE/ULEIS and STEREO-A/SIT.

2.4. Solar Dynamics Observatory

Solar Dynamics Observatory (SDO; W. D. Pesnell et al. 2012) launched on 2010 February 11 into an inclined geosynchronous orbit. For additional context of the solar source of the coronal hole-originating high-speed streams that form SIRs, observations from the Atmospheric Imaging Assembly (AIA; J. R. Lemen et al. 2012) are used. Specifically, the 193 Å channel measurements that encompass both the Fe XII and XXIV lines are used, providing observations of the corona and hot flare plasma, with dark regions denoting coronal holes.

2.5. Event Selection

To select SIR events in observations from all three spacecraft, an analytical time-shifting method was employed following a similar form used in R. C. Allen et al. (2023). The time lag is computed by $\tau = \frac{D_R}{V_R} + \frac{D_T}{V_{T,\mathrm{SIR}} - V_T}$, where D_R and D_T are the radial and transverse RTN components of the vector displacement between ACE/STEREO-A and Solar Orbiter, V_R and V_T are the radial and transverse RTN components of the solar wind velocity vector at ACE/STEREO-A, and $V_{T,\mathrm{SIR}}$ is the tangential rotation rate of SIRs. Following the results of R. C. Allen et al. (2020a), a SIR tangential speed of 14$\overset{\circ}{.}$375 per day is used for $V_{T,\mathrm{SIR}}$, but some deviation from this is expected. The purpose of this time-shifting is to roughly align the observations between spacecraft with more "static" structures in the solar wind. This aids in visually inspecting and matching SIRs, but the subsequent analysis of the particle spectra does not require precisely matched events.

After time-shifting the observations to roughly match that at Solar Orbiter, bulk solar wind and magnetic field observations were used for an initial search of characteristic SIR signatures (see L. Jian et al. 2006; L. K. Jian et al. 2008; R. C. Allen et al. 2020b): (1) a velocity increase, (2) density "pileup" ahead of the velocity increase, (3) tangential flow deflection, (4) increase in the magnetic field magnitude during interval of increasing velocity, and (5) an increase in plasma temperature from the slow to fast speed streams. These cases were further checked to ensure the observations occurred during times of the same polarity of the radial component of the magnetic field to ensure a similar polarity source of solar wind. For context, SDO/AIA 193 Å synoptic maps were used for every potential SIR pairing to allow an understanding of the possibility of multiple, neighboring coronal hole structures. A ballistic footpoint back-mapping (see R. C. Allen et al. 2023) was also applied to ensure a high confidence of a similar source surface location of the high-speed stream. These events were further filtered by those with a dispersionless enhancement in suprathermal particles, a feature typical for a spacecraft sampling prepopulated fluxtubes near SIRs. Finally, events in close proximity to a prior suprathermal particle enhancement (regardless of the cause), in which the particle flux levels had not decayed to background prior to the SIR, were removed.

An example of an SIR observed by all three spacecraft is presented in Figure 1. Synoptic maps of SDO/AIA 193 Å observations (panels (A)–(B)) show a small equatorial hole near Carrington longitudes of ~60° during the two Carrington rotations (CR). During the end of CR 2249 and beginning of CR 2250, STEREO-A, Solar Orbiter, and ACE were near evenly distributed in longitude (Figure 1(C)). All three spacecraft observed the high-speed stream from the coronal hole at ~60°, first arriving at STEREO-A on 2021 October 18, Solar Orbiter on 2021 October 19, and finally, ACE on 2021 October 20. These speed enhancements are concurrent with a tangential flow deflection at both Solar Orbiter and ACE (Figure 1(E)) and follow a density pileup before the rarefaction region (Figure 1(F)). Because public STEREO-A observations only include speed, and not the velocity vector, a tangential flow deflection could not be assessed. The high-speed stream arrival is also concurrent with a solar wind temperature increase at all three spacecraft (Figure 1(G)) and an increase in the magnetic field at STEREO-A and ACE (Figure 1(D)). All of these signatures are indicative of a SIR crossing (see L. Jian et al. 2006; L. K. Jian et al. 2008; R. C. Allen et al. 2020b). Suprathermal ^{4}He intensities are enhanced at the SIR crossing (Figure 1(H)), with lower intensities observed at Solar Orbiter. While the observations at each spacecraft are of a SIR from the same coronal hole source of the high-speed stream, the observed differences may be due to a combination of spatiotemporal variability in the SIR and solar wind, which in this event are deemed to be small enough to include in the study. Additionally, the start of Figure 1, prior to 2021 October 16 at Solar Orbiter and 2021 October 17 at ACE, shows the remaining intensity enhancement from a preceding CME event that erupted on 2021 October 9. For this event, the CME-associated ^{4}He intensity increase is observed to have returned to background levels prior to the SIR-associated enhancement, so it is included in our study. The example event in Figure 1 is shown here as representative of the majority of events included in this study.

When bulk solar wind moments were unavailable, such as in portions of 2020 and early 2021 for Solar Orbiter, then only the suprathermal ion and magnetic field data were used to infer SIR-associated suprathermal particle enhancements. In this case, an increase in the magnetic field magnitude should be observed and the magnetic polarity should match the SIR observations at 1 au with a similar ballistic Carrington longitude. Beyond the magnetic signatures and Carrington longitude alignment with 1 au observations of an SIR, the suprathermal ion observations should be indicative of SIR-associated enhancements, such as low-anisotropy, dispersionless enhancements in ion flux (e.g., C. M. S. Cohen et al. 2020; M. I. Desai et al. 2020; R. C. Allen et al. 2021b). All of these criteria resulted in the identification of 65 initial candidate SIRs for investigation. Prior to investigating potential radial trends with these candidate SIRs, events with clear signs of temporal evolution were removed. This was accomplished both by a

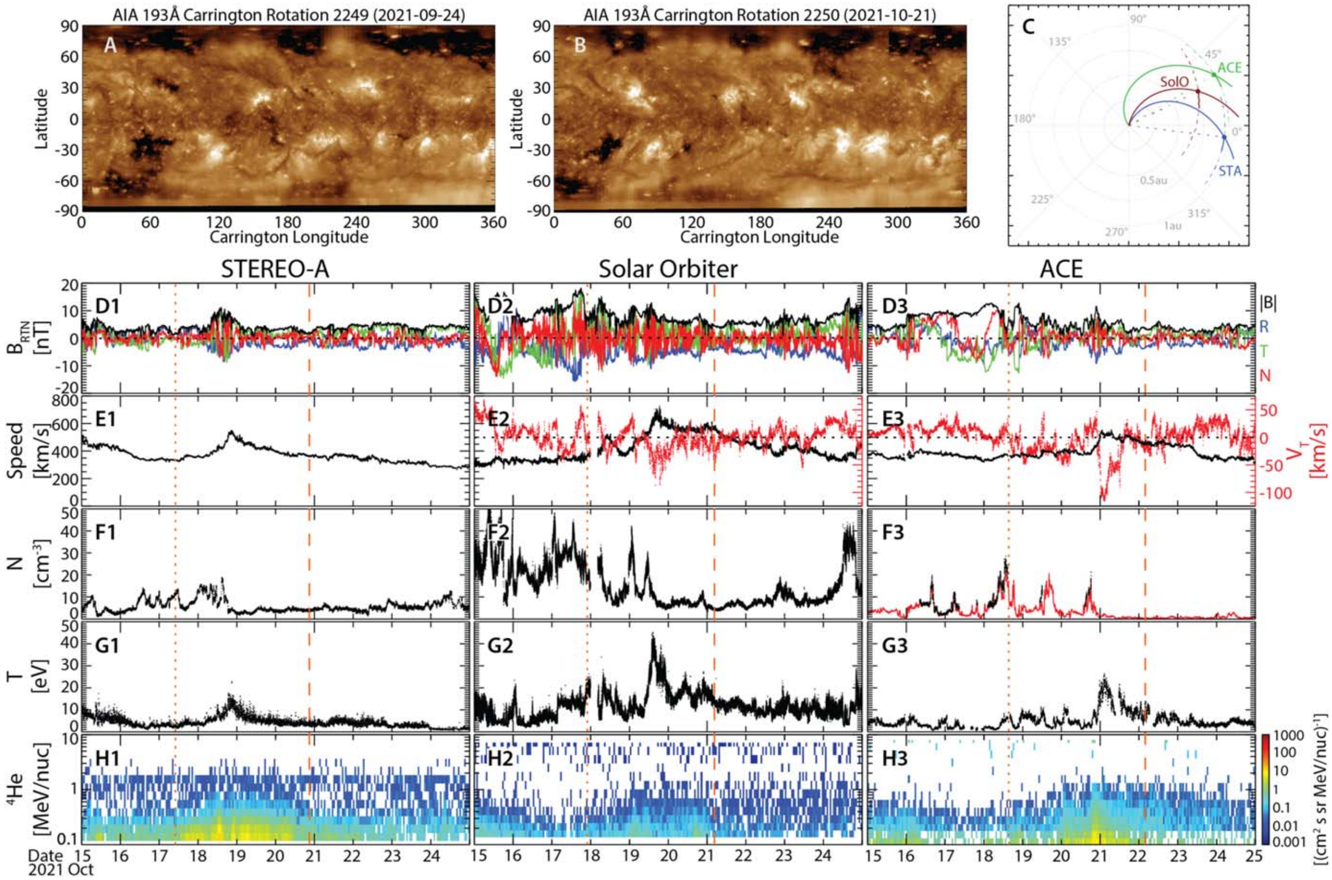

Figure 1. Example of an SIR observed by STEREO-A, Solar Orbiter, and ACE. (A)–(B) SDO/AIA synoptic maps for the two Carrington rotations that correspond to the time period of 2021 October 15–25. (C) Spacecraft locations in the Solar Ecliptic coordinate system with STEREO-A, Solar Orbiter, and ACE in blue, red, and green, respectively. Dashed curves indicate the orbit of the spacecraft for the full duration of the two Carrington rotations in (A) and (B), with the solid curves denoting the spacecraft orbit during the 10 day period shown in rows (D)–(H). For reference, the circles illustrate the spacecraft location on 2021 October 25, with dashed radial lines and Parker Spirals calculated using observed solar wind speeds at each spacecraft. (D1)–(D3) Magnetic field observations in RTN coordinates, (E1)–(E3) solar wind speed (in black) with the tangential solar wind flow, where measured (in red), (F1)–(F3) solar wind density, (G1)–(G3) solar wind temperature, (H1)–(H3) ^{4}He spectrograms. Note that panel (F3) shows both the high-quality data (in black) and the low-latency data (in red) from ACE SWEPAM to provide context to the more sparse high-quality solar wind density data. The dotted (dashed) lines in each column denote the start (stop) time of the suprathermal ion enhancements for that spacecraft.

visual comparison of bulk plasma and magnetic field observations, as well as quantitatively requiring that the radial comparison of fluences, J, between Solar Orbiter and ACE/STEREO-A was dominant over the longitudinal comparison of fluences between ACE and STEREO-A (i.e., $J_{\rm SolO}/J_{\rm ACE} < J_{\rm STA}/J_{\rm ACE}$ and $J_{\rm SolO}/J_{\rm STA} < J_{\rm ACE}/J_{\rm STA}$), which placed a further constraint that the SIR be observed by all three spacecraft. Additionally, the maximum time lag between the observation at Solar Orbiter and the nearest in time observation from 1 au was 7 days, further reducing the impacts of potential temporal evolution. Finally, only fluences with uncertainty less than 25% were included in this study. This additional filtering resulted in 34 events deemed suitable for study (listed in Table 1). Three of these events have associated shocks at 1 au, which is also indicated in Table 1. These candidate SIRs can be seen in Figure 2, which shows the full time span of the study, with the ACE and STEREO-A measurements time-shifted to events observed by Solar Orbiter.

3. Results

Rigidity is the natural unit to frame questions of particle diffusion, and it is also the more fundamental quantity for investigating particle transport into the heliosphere (e.g., J. F. Valdes-Galicia 1993; J. W. Bieber et al. 1994; A. Shalchi et al. 2004; M. Hussein & A. Shalchi 2016). As such, the particle energies observed by Solar Orbiter, ACE, and STEREO-A are converted into rigidity space using the conversion outlined in the review by D. V. Reames (1999). In this formulation, the rigidity, P, is defined by

$$P = \frac{pc}{\mathrm{Q}e} = \frac{M_u \beta\gamma \mathrm{A}}{\mathrm{Q}}, \tag{3}$$

where p is particle momentum, Q is the ionic charge number, e is the charge of an electron, $\beta = v/c$ is the particle velocity relative to the speed of light, $\gamma = (1-\beta^2)^{-1/2}$, A is the atomic mass, and $M_u = m_u c^2 = 931.494$ is the proton mass in units of [MeV/c^2]. Since ACE/ULEIS, STEREO-A/SIT, and Solar Orbiter/SIS do not measure the particle charge state, average charge states are assumed (i.e., 2, 6.05, 9.84 for ^{4}He, O, and Fe, respectively) based on previous studies (e.g., R. von Steiger et al. 2000; R. J. Filwett et al. 2019).

Only the fluence ratios for the nearest in time spacecraft comparisons (Solar Orbiter to ACE or Solar Orbiter to STEREO-A) were used to investigate radial trends per SIR event (Figure 3 and Table 2) to reduce temporal effects without

Table 1
SIR-associated Suprathermal Particle Enhancements Passing Filtering Criteria in Text

Event Number	Solar Orbiter Observations Start Time (UT)	Duration (hr)	Distance (au)	Observations at 1 au Matching Spacecraft	Start Time (UT)	Duration (hr)
1[a]	2020-04-23/09:40	26.0	0.78	ACE	2020-04-21/05:00	99.3
2	2020-05-01/20:00	127.0	0.71	ACE	2020-05-02/09:00	51.0
3	2020-05-19/04:00	60.0	0.61	ACE	2020-05-20/09:00	51.0
4	2020-07-01/11:00	139.0	0.57	ACE	2020-06-27/07:00	109.0
5	2020-12-24/21:00	50.0	0.74	ACE	2020-12-22/02:30	48.5
6[a]	2021-01-12/10:00	85.5	0.61	ACE	2021-01-09/22:30	65.0
7	2021-02-17/16:00	46.5	0.51	STEREO-A	2021-02-21/08:30	67.5
8	2021-03-07/19:00	49.5	0.60	ACE	2021-03-13/08:00	89.5
9	2021-03-18/16:30	28.5	0.67	STEREO-A	2021-03-20/19:00	88.3
10	2021-03-25/17:00	35.0	0.72	STEREO-A	2021-03-30/16:30	22.0
11	2021-04-03/23:00	31.5	0.77	STEREO-A	2021-04-02/04:00	22.0
12	2021-04-06/09:00	102.0	0.80	STEREO-A	2021-04-10/06:00	110.0
13	2021-04-13/07:30	87.5	0.83	STEREO-A	2021-04-16/11:30	38.0
14	2021-04-18/11:00	51.0	0.85	STEREO-A	2021-04-20/09:30	128.5
15	2021-04-25/14:00	44.0	0.88	STEREO-A	2021-04-30/09:00	29.0
16	2021-05-04/10:30	41.0	0.91	STEREO-A	2021-05-08/08:30	21.5
17	2021-05-31/03:00	33.0	0.95	STEREO-A	2021-06-03/22:30	55.5
18	2021-06-11/11:00	131.0	0.96	STEREO-A	2021-06-11/18:00	102.0
19	2021-07-03/06:00	68.5	0.90	STEREO-A	2021-07-07/23:00	60.0
20	2021-08-02/01:30	25.5	0.76	STEREO-A	2021-08-05/15:00	147.0
21	2021-08-21/02:00	57.5	0.64	STEREO-A	2021-08-24/02:00	79.0
22	2021-09-08/16:30	52.0	0.59	STEREO-A	2021-09-07/06:00	63.0
23	2021-09-25/02:30	36.0	0.61	STEREO-A	2021-09-25/19:30	53.0
24	2021-10-02/15:30	56.5	0.65	STEREO-A	2021-10-06/22:00	17.0
25	2021-10-17/22:00	78.5	0.72	STEREO-A	2021-10-17/10:00	83.0
26	2021-11-15/05:00	74.0	0.93	ACE	2021-11-15/19:00	36.0
27	2021-12-18/04:00	144.0	1.01	STEREO-A	2021-12-17/18:00	45.5
28	2022-01-24/17:30	22.0	0.90	STEREO-A	2022-01-24/00:00	44.0
29	2022-02-18/07:00	108.0	0.68	ACE	2022-02-18/12:00	162.0
30	2022-03-24/15:00	13.5	0.32	ACE	2022-03-22/22:00	20.0
31	2022-03-28/18:30	92.0	0.34	ACE	2022-03-27/04:00	47.5
32	2022-10-16/05:30	158.5	0.33	STEREO-A	2022-10-21/23:30	190.0
33[a]	2022-11-22/15:00	98.5	0.75	ACE	2022-11-20/16:30	105.0
34	2022-12-07/13:30	133.0	0.87	STEREO-A	2022-12-07/18:00	147.5

Note.
[a] Shock observed at 1 au.

double counting events. A power-law fit ($J_{\rm obs}/J_{1\,\rm au} = r^{\gamma}$) was computed using least-squares regression (dashed lines in Figure 3) and compared to the radial dependence expected from L. A. Fisk & M. A. Lee (1980) assuming a shock location beyond 1 au (red lines in Figure 3). As Figure 3 compares the relative fluence (i.e., $J_{\rm obs}/J_{1\,\rm au}$), the location of the SIR-driven shock outside of 1 au does not change the anticipated slope in the L. A. Fisk & M. A. Lee (1980) framework. Events with an associated shock at 1 au, for which additional dynamics may be impacting the relative fluence beyond just transport, are indicated with a red circle. While some of the species and rigidities show agreement between the slope expected from L. A. Fisk & M. A. Lee (1980) and the fitted power law, these are typically limited to those with less radial range in observations (i.e., O at 54.31 MV). There is, however, a notable scatter in the observed relative fluence. Some potential causes for deviation from the power-law fit include smaller temporal evolution and/or latitudinal variations between spacecraft, distributions of charge states impacting the conversion to rigidity space, mesoscale structuring of the SIR, higher order impacts of transport of the normalized abundance of particles, or varying degrees of local compressive acceleration (e.g., N. A. Schwadron et al. 1996; J. Giacalone et al. 2002; R. J. Filwett et al. 2017, 2019; R. C. Allen et al. 2020b). However, there is an insufficient number of events to conclusively investigate the causes of variations from the power-law fits at this time.

The power-law exponent from the fits in Figure 3, along with the exponent from the less than 1 au events in M. A. I. Van Hollebeke et al. (1978), are shown versus rigidity in Figure 4(a). The dotted line in Figure 4(a) shows the power-law fit ($\gamma = 1.15P^{-0.35}$) of all observations of this study plus that from M. A. I. Van Hollebeke et al. (1978). Figure 4(a) also includes curves for the expected relationship from L. A. Fisk & M. A. Lee (1980) for each species. The profiles for L. A. Fisk & M. A. Lee (1980) are derived assuming the shock is outside 1 au with parameters from G. M. Mason et al. (1999), i.e., $\beta = 4$, $\kappa_0 = 6.67 \times 10^{-2}$, and $V = 800\ \rm km\ s^{-1}$ in Equation (1). Several species are within error of the L. A. Fisk & M. A. Lee (1980) trends (i.e., protons from M. A. I. Van Hollebeke et al. 1978 and

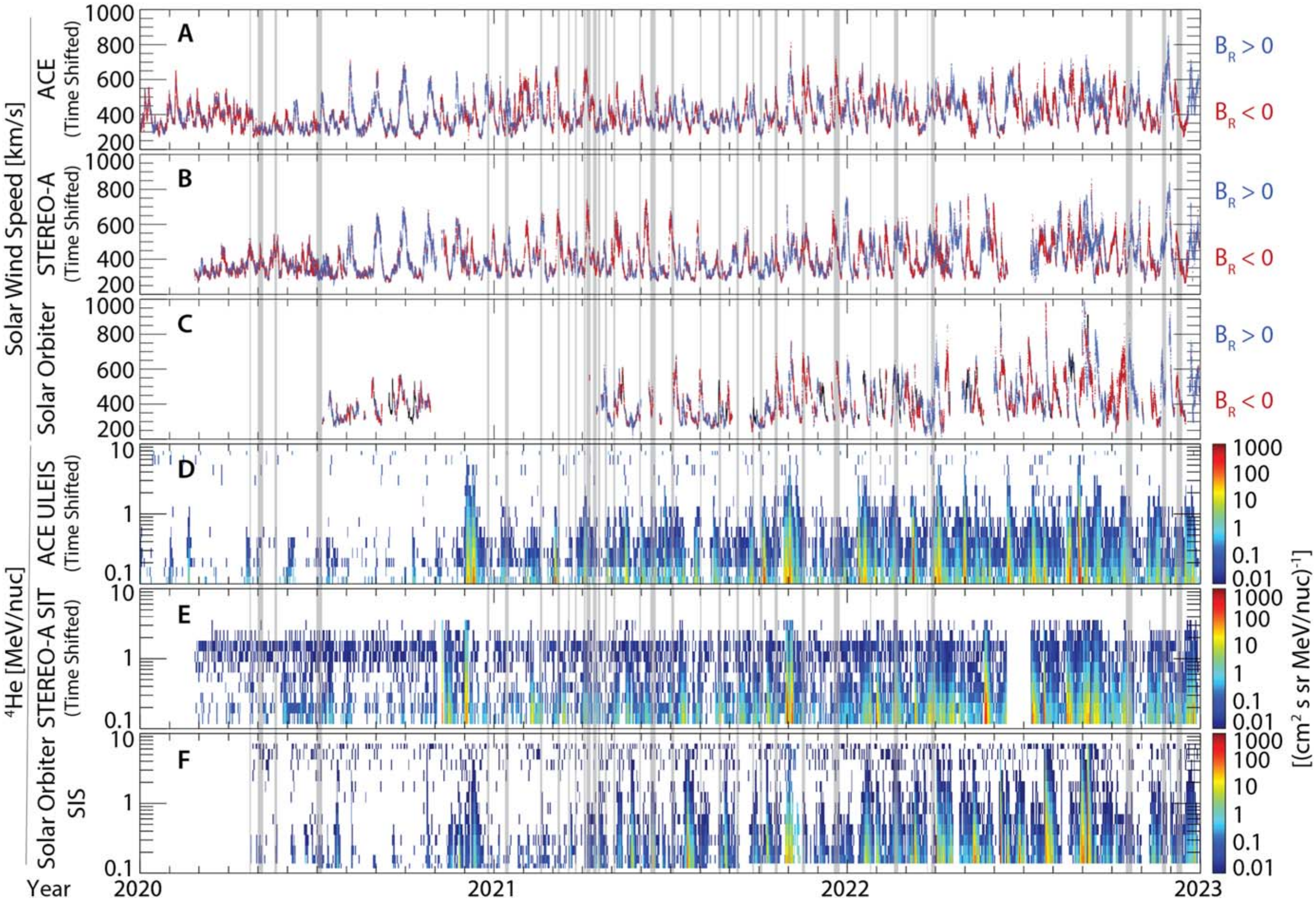

Figure 2. Three years of observations from ACE, STEREO-A, and Solar Orbiter, averaged down to 30 minute resolution, showing ((A)–(C)) solar wind speed colored by magnetic polarity (blue is positive B_R, red is negative B_R, and black indicates time without public magnetic field data at time of publication), and ((D)–(F)) 1 hr averaged suprathermal ^{4}He flux. Data resolution was reduced solely for the purpose of displaying three years of observations. Gray vertical bars denote the 33 intervals of SIR-associated suprathermal ion flux increases at Solar Orbiter that corresponded to suprathermal flux increases at ACE and STEREO-A, meeting all criteria defined in the text. Note, the apparent gap in STEREO-A observation from mid-June through early 2022 July is an artifact from time-shifting.

the one data point with a sufficient number of oxygen observations). However, the iron and ^{4}He observations deviate from the L. A. Fisk & M. A. Lee (1980) expectations. Further, the ^{4}He γ, which have the most number of samples and were fitted from a population with a larger radial diversity, are above the oxygen and Fe γ at similar rigidities. This runs counter to the expected trend from L. A. Fisk & M. A. Lee (1980), which would have the ^{4}He slopes less than those for heavier ions at similar rigidities.

Along with investigating the radial slopes of the relative fluence by rigidity, Figure 4(b) illustrates these slopes as a function of particle velocity, which is the only other parameter available in Equation (1). As in Figure 4(a), the oxygen and proton observations are found to more closely follow the L. A. Fisk & M. A. Lee (1980) dependence. In particle velocity space, there is no mass dependence to the expected radial profiles of particle fluence in L. A. Fisk & M. A. Lee (1980). However, all ^{4}He slopes fall above that expected by L. A. Fisk & M. A. Lee (1980), signifying a stronger decrease in fluence with increasing radial separation for ^{4}He than expected for all particle velocities, with all but one ^{4}He γ being within a factor of 2 from predicted by L. A. Fisk & M. A. Lee (1980) (dotted curve in Figure 4(b)). Further, the Fe γ values fall below that predicted from L. A. Fisk & M. A. Lee (1980), signifying less fluence decrease than estimated.

4. Discussion

This study investigates the radial variation in normalized SIR-associated suprathermal particle fluence as a function of rigidity. The main finding is that the power-law exponents of the normalized fluence in the inner heliosphere, γ, follow roughly a power-law trend ($\gamma = 1.15P^{-0.35}$). Applying this empirical relationship, a comparison to the theoretical variation of particle spectra can be performed. Figure 5 shows this comparison between the variation of particle spectra from a SIR-driven shock at different radial distances when viewed from 1 au following the framework in L. A. Fisk & M. A. Lee (1980) and that derived from observations in this study. The general modulation of the particle spectra is similar, i.e., greater loss of lower energy populations than higher energy populations, but the modulation from the empirical relationship found in this study is less extreme than predicted by the equations of L. A. Fisk & M. A. Lee (1980). Even for shocks beyond 6 au, the observations here indicate that a spectral rollover will still not be clearly observed. This could be due to multiple reasons, including sub-Parker spiral magnetic field configurations or the treatment of the velocity-dependent diffusion term in L. A. Fisk & M. A. Lee (1980).

Sub-Parker spiral magnetic fields can result from magnetic footpoint movement at the coronal hole boundary leading to a more radial magnetic field behind SIRs (N. Murphy et al. 2002;

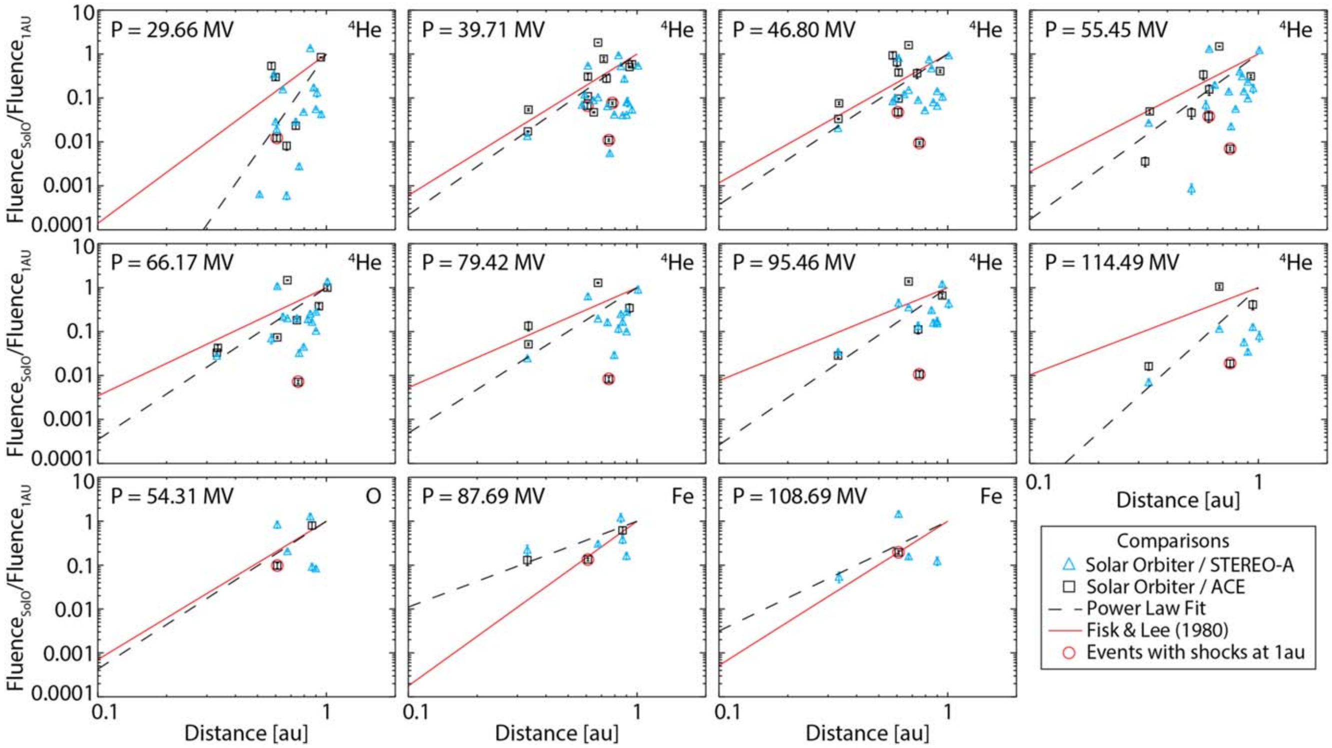

Figure 3. Normalized fluence decrease ($J_{\mathrm{obs}}/J_{1\ \mathrm{au}}$) as a function of Solar Orbiter radial distance for different bins of rigidity for ^{4}He (top and middle rows), O, and Fe (bottom row). Comparisons between Solar Orbiter and ACE are shown as black squares, while those between Solar Orbiter and STEREO-A are shown as blue triangles. Events with an observed shock at 1 au are circled in red. Power-law fits are shown with the dashed black line for each rigidity bin, and the expected slope from L. A. Fisk & M. A. Lee (1980), assuming a shock beyond 1 au, is shown in red.

Table 2
Power-law Fit Parameters from Figure 3

Rigidity (MV)	Species	γ
29.66	^{4}He	7.438 ± 0.311
39.71	^{4}He	3.708 ± 0.206
46.80	^{4}He	3.466 ± 0.209
54.31	O	3.371 ± 0.542
55.45	^{4}He	3.791 ± 0.184
66.17	^{4}He	3.478 ± 0.249
79.42	^{4}He	3.328 ± 0.260
87.69	Fe	1.957 ± 0.269
95.46	^{4}He	3.603 ± 0.338
108.69	Fe	2.501 ± 0.339
114.49	^{4}He	4.728 ± 0.377

C. J. Joyce et al. 2021; N. A. Schwadron et al. 2021). The effect of such a configuration is a shorter path length between the observer and the SIR-driven shock than along the normal Parker spiral. This would lessen the effects of transport-driven modulation of the observed particle spectra and may result in the empirical relationship of this study being more consistent with an L. A. Fisk & M. A. Lee (1980) spectrum at a shorter distance from the SIR-driven shock.

Another possibility is that the treatment of the diffusion term ($\kappa = \kappa_0 v r$) in L. A. Fisk & M. A. Lee (1980) does not fully account for species-dependent processes. G. Li et al. (2009) postulated that the velocity term in the diffusion coefficient term at CMEs should be instead characterized as being proportional to v^{λ} rather than solely proportional to v. It is possible that a rederivation of the L. A. Fisk & M. A. Lee (1980) equations with this different treatment of the diffusion coefficient would alter the anticipated particle spectra modulation, and so would be more comparable to the empirical relationship of this study. This would be similar to simulation results on the impacts of variations to the cross-diffusion coefficients on seed populations resulting from high-speed streams (N. Wijsen et al. 2023). The lower degree of particle spectra modulation of this study, however, is consistent with studies close to the Sun without a clear spectral rollover (e.g., G. Gloeckler et al. 1979; K. Chotoo et al. 2000; M. I. Desai et al. 2020; R. C. Allen et al. 2021a; C. J. Joyce et al. 2021).

We note, however, that one source of uncertainty in this analysis is the need to assume a charge state for each species. While average thermal charge states are used in this study (i.e., $^4He^{2+}$, $O^{6.05+}$, and $Fe^{9.84+}$; see, e.g., R. von Steiger et al. 2000; R. J. Filwett et al. 2019), the true average charge state may vary from event to event. Similarly, as the SIR-associated suprathermal particles are accelerated further out in the heliosphere, there may be a nonnegligible abundance of accelerated pick-up $^4He^{+}$ within the SIR (K. Chotoo et al. 2000; M. H. Walker et al. 2025). However, using a lower average charge state of ^{4}He will increase the rigidity of ^{4}He, which would shift the observed normalized flux decrease further from that derived from the L. A. Fisk & M. A. Lee (1980) formulation.

While more SIR events would constrain statistical variations for particles of different rigidities, solar activity has increased as the solar cycle approaches maximum, making investigations of isolated SIRs more challenging. However, future investigations of SIRs will be using observations as Solar Orbiter moves further out of the ecliptic. These future observations will aid in our understanding of latitudinal variations of SIR-associated

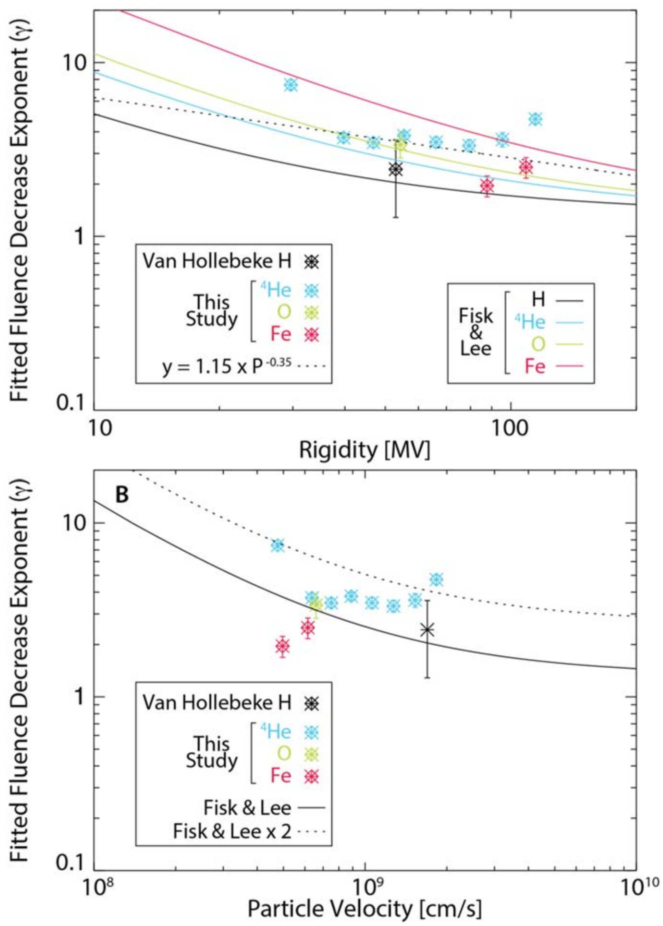

Figure 4. (A) Power-law exponents of normalized fluence vs. radial separation from the fits in Figure 3 as a function of rigidity (blue, green, and red points for ^{4}He, O, and Fe, respectively), including the power-law exponent of normalized peak proton intensity vs. radial separation from observations in M. A. I. Van Hollebeke et al. (1978) at less than 1 au (black point). The dashed line is the power-law fit through all data points shown. The solid curves are the expected values derived from the L. A. Fisk & M. A. Lee (1980) formulation for each species noted. (B) Same as in panel (A), but as a function of particle velocity. The solid black curve shows the expected values of power-law exponents as a function of particle velocity from L. A. Fisk & M. A. Lee (1980), which does not include species-dependent terms.

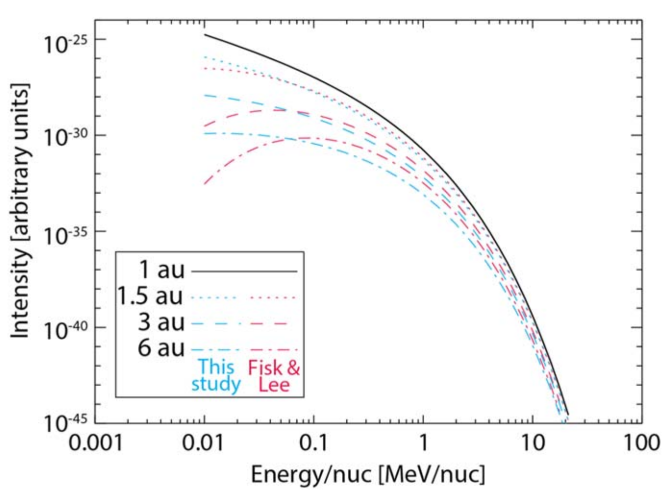

Figure 5. Comparison of the spectral modulation from L. A. Fisk & M. A. Lee (1980) (in red) with the empirically derived spectra in this study (in blue) for shocks at various radial distances when viewed from 1 au.

suprathermal particle fluences. Along with more events for improved counting statistics per ion species, this improved understanding may allow for better refinement of the empirical relationship of this study.

Acknowledgments

Solar Orbiter is a mission of international cooperation between ESA and NASA, operated by ESA. The Suprathermal Ion Spectrograph (SIS) is a European facility instrument funded by ESA during construction, and NASA funds the instrument during Phase E operation. Solar Orbiter postlaunch work at SwRI and JHU/APL is supported by NASA contract 80GFSC25CA035, and we thank NASA headquarters and the NASA/GSFC Solar Orbiter project office for their continuing support. J.R.P. acknowledges the financial support by the Spanish Ministerio de Ciencia, Innovación y Universidades FEDER/MCIU/AEI Projects ESP2017-88436-R and PID2019- 104863RB-I00/AEI/10.13039/501100011033. R.F.W.S. thanks ESA for supporting the build of SIS under contract number SOL.ASTR.CON.00004; the German Federal Ministry for Economic Affairs and Energy and the German Space Agency (Deutsches Zentrum für Luft- und Raumfahrt, e.V., (DLR)) for their unwavering support under grant Nos. 50OT0901, 50OT1202, 50OT1702, and 50OT2002; and the University of Kiel and the Land Schleswig-Holstein for their support of SIS. R.C.A. and G.L. acknowledge support from NASA grant 80NSSC21K0733. R.C.A., G.L., R.J.F., and M.D. additionally thank NASA grant 80NSSC24K0908. R.C.A. and S.K.V. acknowledge support from NASA grant 80NSSC22K0993.

ORCID iDs

Robert C. Allen https://orcid.org/0000-0003-2079-5683
George C. Ho https://orcid.org/0000-0003-1093-2066
Glenn M. Mason https://orcid.org/0000-0003-2169-9618
Athanasios Kouloumvakos https://orcid.org/0000-0001-6589-4509
Gang Li https://orcid.org/0000-0003-4695-8866
Rachael J. Filwett https://orcid.org/0000-0002-5497-7867
Maher Dayeh https://orcid.org/0000-0001-9323-1200
Malik H. Walker https://orcid.org/0000-0003-4380-3519
Sarah K. Vines https://orcid.org/0000-0002-7515-3285
Robert F. Wimmer-Schweingruber https://orcid.org/0000-0002-7388-173X
Javier Rodriguez-Pacheco https://orcid.org/0000-0002-4240-1115

References

Acuña, M. H., Curtis, D., Scheifele, J. L., et al. 2008, SSRv, 136, 203
Allen, R. C., Gibson, S. E., Hewins, I., et al. 2023, JGRA, 128, e2023JA031361
Allen, R. C., Ho, G. C., Jian, L. K., et al. 2020a, SpWea, 18, e02437
Allen, R. C., Ho, G. C., Mason, G. M., et al. 2021a, GeoRL, 48, e91376
Allen, R. C., Lario, D., Odstrcil, D., et al. 2020b, ApJS, 246, 36
Allen, R. C., Mason, G. M., Ho, G. C., et al. 2021b, A&A, 656, L2
Bieber, J. W., Matthaeus, W. H., Smith, C. W., et al. 1994, ApJ, 420, 294
Chotoo, K., Schwadron, N. A., Mason, G. M., et al. 2000, JGR, 105, 23107
Cohen, C. M. S., Christian, E. R., Cummings, A. C., et al. 2020, ApJS, 246, 20
Desai, M. I., Mitchell, D. G., Szalay, J. R., et al. 2020, ApJS, 246, 56
Filwett, R. J., Desai, M. I., Dayeh, M. A., & Broiles, T. W. 2017, ApJ, 838, 23
Filwett, R. J., Desai, M. I., Ebert, R. W., & Dayeh, M. A. 2019, ApJ, 876, 88
Fisk, L. A., & Lee, M. A. 1980, ApJ, 237, 620
Galvin, A. B., Kistler, L. M., Popecki, M. A., et al. 2008, SSRv, 136, 437
Giacalone, J., Jokipii, J. R., & Kóta, J. 2002, ApJ, 573, 845
Gloeckler, G., Hovestadt, D., & Fisk, L. A. 1979, ApJL, 230, L191
Henderson, S. A., Filwett, R. J., Allen, R. C., et al. 2025, ApJ, 981, 87

Horbury, T. S., O'Brien, H., Carrasco Blazquez, I., et al. 2020, A&A, 642, A9
Hussein, M., & Shalchi, A. 2016, ApJ, 817, 136
Jian, L., Russell, C. T., Luhmann, J. G., & Skoug, R. M. 2006, SoPh, 239, 337
Jian, L. K., Russell, C. T., Luhmann, J. G., Skoug, R. M., & Steinberg, J. T. 2008, SoPh, 250, 375
Joyce, C. J., McComas, D. J., Schwadron, N. A., et al. 2021, A&A, 650, L5
Kaiser, M. L., Kucera, T. A., Davila, J. M., et al. 2008, SSRv, 136, 5
Lemen, J. R., Title, A. M., Akin, D. J., et al. 2012, SoPh, 275, 17
Li, G., Zank, G. P., Verkhoglyadova, O., et al. 2009, ApJ, 702, 998
Luhmann, J. G., Curtis, D. W., Schroeder, P., et al. 2008, SSRv, 136, 117
Mason, G. M., Gold, R. E., Krimigis, S. M., et al. 1998, SSRv, 86, 409
Mason, G. M., Korth, A., Walpole, P. H., et al. 2008, SSRv, 136, 257
Mason, G. M., von Steiger, R., Decker, R. B., et al. 1999, SSRv, 89, 327
McComas, D. J., Bame, S. J., Barker, P., et al. 1998, SSRv, 86, 563
Müller, D., St. Cyr, O. C., Zouganelis, I., et al. 2020, A&A, 642, A1
Murphy, N., Smith, E. J., & Schwadron, N. A. 2002, GeoRL, 29, 2066
Owen, C. J., Bruno, R., Livi, S., et al. 2020, A&A, 642, A16
Pesnell, W. D., Thompson, B. J., & Chamberlin, P. C. 2012, SoPh, 275, 3
Pizzo, V. 1978, JGR, 83, 5563
Reames, D. V. 1999, SSRv, 90, 413
Richardson, I. G. 2004, SSRv, 111, 267
Rodríguez-Pacheco, J., Wimmer-Schweingruber, R. F., Mason, G. M., et al. 2020, A&A, 642, A7
Schwadron, N. A., Fisk, L. A., & Gloeckler, G. 1996, GeoRL, 23, 2871
Schwadron, N. A., Joyce, C. J., Aly, A., et al. 2021, A&A, 650, A24
Shalchi, A., Bieber, J. W., Matthaeus, W. H., & Qin, G. 2004, ApJ, 616, 617
Smith, C. W., L'Heureux, J., Ness, N. F., et al. 1998, SSRv, 86, 613
Stone, E. C., Frandsen, A. M., Mewaldt, R. A., et al. 1998, SSRv, 86, 1
Valdes-Galicia, J. F. 1993, SSRv, 62, 67
Van Hollebeke, M. A. I., McDonald, F. B., Trainor, J. H., & von Rosenvinge, T. T. 1978, JGR, 83, 4723
von Steiger, R., Schwadron, N. A., Fisk, L. A., et al. 2000, JGRA, 105, 27217
Walker, M. H., Allen, R. C., Li, G., et al. 2025, A&A, 693, A230
Wijsen, N., Li, G., Ding, Z., et al. 2023, JGRA, 128, e2022JA031203
Wimmer-Schweingruber, R. F., Janitzek, N. P., Pacheco, D., et al. 2021, A&A, 656, A22
Yu, J., Berger, L., Drews, C., Wimmer-Schweingruber, R., & Taut, A. 2018, A&A, 615, A126
Yu, J., Berger, L., Wimmer-Schweingruber, R., et al. 2017, A&A, 599, A13
Zhao, L., Li, G., Ebert, R. W., et al. 2016, JGRA, 121, 77